Atmos. Chem. Phys. Discuss., 12, 9451–9490, 2012
www.atmos-chem-phys-discuss.net/12/9451/2012/
doi:10.5194/acpd-12-9451-2012

Atmospheric Chemistry and Physics Discussions

Overview of aerosol properties associated with air masses sampled by the ATR-42 during the EUCAARI campaign (2008)

S. Crumeyrolle[1], A. Schwarzenboeck[1], K. Sellegri[1], J. F. Burkhart[2], A. Stohl[2], L. Gomes[3], B. Quennehen[1], G. Roberts[3], R. Weigel[1,4], J. C. Roger[1], P. Villani[1,5], J. M. Pichon[1], T. Bourrianne[3], and P. Laj[1,5]

[1]Laboratoire de Météorologie Physique, CNRS, Université Blaise Pascal, UMR6016, Clermont-Ferrand, France
[2]Norwegian Institute for Air Research, Kjeller, Norway
[3]Centre National de Recherches Météorologiques, Météo-France, Toulouse, France
[4]Institute for Physics of the Atmosphere, Johannes Gutenberg University, Mainz, Germany
[5]Laboratoire de Glaciologie et Géophysique de l'Environnement, Université de Grenoble, CNRS, Grenoble, France

Received: 20 March 2012 – Accepted: 23 March 2012 – Published: 12 April 2012

Correspondence to: S. Crumeyrolle (suzanne.crumeyrolle@gmail.fr)

Published by Copernicus Publications on behalf of the European Geosciences Union.

Abstract

Within the frame of the European Aerosol Cloud Climate and Air Quality Interactions (EUCAARI) project the Météo-France aircraft ATR-42 performed 22 research flights, over central Europe and the North Sea during the intensive observation period in May 2008. For the campaign, the ATR-42 was equipped in order to study aerosol physical, chemical and optical properties, as well as cloud microphysics. During the campaign, continental air masses from Eastern and Western Europe were encountered, along with polar and Scandinavian air masses. For the 22 research flights, retroplume analyses along the flight tracks were performed with FLEXPART in order to classify air masses into five sectors of origin which allows for a qualitative evaluation of emission influence on the respective air parcel.

In the polluted boundary layer (BL), typical concentrations of particles with diameters larger than 10 nm (N_{10}) are of the order of 5000–6000 cm^{-3}, whereas N_{10} concentrations of clean air masses were lower than 1300 cm^{-3}. The detection of the largest particle number concentrations occurred in air masses coming from Polar and Scandinavian regions for which an elevated number of nucleation mode (25–28 nm) particles was observed and attributed to new particle formation over open sea. In the free troposphere (FT), typical observed N_{10} are of the order of 900 cm^{-3} in polluted air masses and 400–600 cm^{-3} in clean air masses, respectively. In both layers, the chemical composition of submicron aerosol particles is dominated by organic matter and nitrate in polluted air masses, while, sulphate and ammonium followed by organics dominate the submicron aerosols in clean air masses. The highest CCN/CN ratios were observed within the polar air masses while the CCN concentration values are the highest within the polluted air masses.

Within the five air mass sectors defined and the two layers (BL and FT), observations have been distinguished into anticyclonic (first half of May 2008) and cyclonic conditions (second half of May 2008). Strong relationships between meteorological conditions and physical, chemical as well as optical properties are found.

ACPD

12, 9451–9490, 2012

1 Introduction

Aerosols are known to have significant impact on the regional and global climate via interaction with the solar and terrestrial radiation, thereby modifying the planetary albedo and the outgoing longwave radiation (IPCC, 2007). Aerosols originate either from natural sources or emission by anthropogenic activities (e.g. mineral dust, sea salt, black carbon, sulfate, biomass burning smoke, biogenic aerosols). During the longrange transport, aerosol particles may influence the climate by interfering directly with the atmospheric radiative processes (Haywood et al., 2003; IPCC, 2007) and indirectly by modifying the distribution of clouds (Lohmann et al., 2004). All these direct and indirect effects depend on aerosol particle properties: concentration, size, chemical composition, hygroscopic properties, mixing state (Roberts et al., 2001; Wang et al., 2011).

The contributions of the various aerosol sources, the role of long-range transport, and the contributions of primary and secondary particulate matter to the atmospheric aerosol concentrations over Europe are still not well quantified. The aerosol parameters influencing the radiative balance and the properties of clouds remain particularly uncertain (Adams and Seinfeld, 2002; Kaufman et al., 2002; Spichtinger and Cziczo, 2008). Moreover, Europe is under the influence of polluted air masses, from industrial country, as well as clean air masses from polar regions. The mixing of these different types of air mass may lead to a regional mixed plume with modified properties compared to the non-mixed plumes. In particular the atmospheric residence time of pollution and the radiative effect of pollution aerosols are expected to be modified (Andrea and Crutzen, 1997).

This study presents results from an intensive airborne measurement campaign, carried out over Netherlands as part of the EUCAARI (European Aerosol Cloud Climate and Air Quality Interactions) project (Kulmala et al., 2009). The airborne measurement campaign include the deployment of five European instrumented research aircraft (German DLR Falcon-20, the British FAAM Bae-146 and NERC Dornier, and the French ATR-42 and Falcon-20 from Météo-France) was performed in May 2008.

ACPD
12, 9451–9490, 2012

Here we focus on aerosol physical and chemical properties which were performed simultaneously with optical measurements onboard the French ATR-42. This characterisation encompasses measurement of the number size distribution, hygroscopicity, volatility, scattering coefficient and chemical component. During the campaign a variety of clean marine and polluted continental air masses were encountered and some of the key aerosol properties associated with these particular air masses are documented and reported here. Moreover, distinct layers, such as the boundary layer and the free troposphere, could be sampled during the same flight and over different surface types (land/sea), almost simulataneously. The results of that kind of investigation are likely to be of significant interest to both the process-modelling community and the large-scale modeling community.

2 Aircraft and instrumentation

To improve our understanding of processes related to atmospheric aerosol physics and chemistry, from aerosol nanometer size scale to the overall aerosol-cloud-climate scale (i.e. millimeter size), the French ATR-42 research aircraft performed a total of 22 research flights between 2 May and 30 May 2008. The ATR-42 operated by SAFIRE (Service des Avions Francais Instrument pour la Recherche en Environnement) was based at Rotterdam airport in the Netherlands for the duration of the EUCAARI intensive observation period. The 22 research flights have been grouped into six different types of flights, according to flight plans, as described in Crumeyrolle et al. (2010). Fourteen (RF42, RF44, RF47, RF49, RF51, RF52, RF55, RF56, RF57, RF58, RF59, RF60, RF62, RF63) over the 22 flights performed during the campaign have been used in this study while the other eight flights were dedicated to observation of new particle formation events Crumeyrolle et al. (2010).

The instrumental payload of the French research aircraft ATR-42 has been particularly designed to aerosol-cloud interaction studies as partially discussed in previous studies (Crumeyrolle et al., 2008; Matsuki et al., 2010). The aerosol instrumentation

ACPD
12, 9451–9490, 2012

performed the particle sampling via the ATR-42 community aerosol inlet (CAI). The isokinetic (and isoaxial) CAI, based on the construction by the University of Hawaï equipped with a shrouded solid diffuser inlet designed by A. Clarke and modified by Meteo France, has a 50 % sampling efficiency ($Dp_{50\,\%}$ for particle diameter around 5 µm (McNaughton et al., 2007, Gomes et al., in preparation). Two condensation particle counters (CPC, TSI model 3025 and 3010; McMurry, 2000) were used to measure total ambient aerosol concentrations (N_3 and N_{10} respectively). The 50 % detection diameter is 3 and 10 nm for each CPC, respectively (Mertes et al., 1995; Stoltzenburg and McMurry, 1991).

A scanning mobility particle sizer (SMPS) was used to measure the number size distribution of aerosol particles with diameters from 0.02 to 0.5 µm. This instrument consisted of a differential mobility analyzer (DMA) as described by Villani et al. (2007) and a CPC (TSI model 3010) for particle detection downstream the DMA. The DMA sheath flow rate was controlled with a critical orifice in a closed loop arrangement (Jokinen and Mäkelä, 1996). Typically the scan time – yielding one complete number size distribution - was chosen to be 90 s. In parallel, there was another set of SMPS and optical particle counter (OPC) measuring particles downstream of a thermo-desorption column wherein the particles were heated up to 280 °C. Comparison of the non conditioned and heated total aerosol spectra provides indirect information on the bulk aerosol composition. Particles "surviving" after being heated to 280 °C are denoted as refractory particles (e.g. sea salt, soot, mineral dust), otherwise the particles should be mainly composed of volatile species (e.g. ammonium nitrate, ammonium sulphate and some organic compounds).

The Cloud Condensation Nuclei Counter (CCNC) used in this study was a continuous-flow streamwise thermal-gradient CCN counter, commercially available from Droplet Measurement Technologies, Inc. (DMT, model No. CCN-100). The design and operating principles of the instrument are based on Roberts and Nenes (2005). The aerosol sample enters the column at the top center of the column, and particles with a critical supersaturation less than the centerline supersaturation are activated as

ACPD
12, 9451–9490, 2012

CCN. The residence time in the column (612 s, depending on flow rate) enables the activated particles to grow to droplets that are sufficiently large (>1 µm) to be detected separately from unactivated particles (usually <1 µm). An OPC at the exit of the column determines the concentration and size distribution of droplets in the size range of 0.75–10 µm. Droplets larger than 1 µm are considered to be activated CCN. The supersaturation was set at 0.2 % during the whole field campaign.

A Time of Flight Aerosol Mass Spectrometer (C-ToF-AMS; Drewnick et al., 2005; Canagaratna et al., 2007) was used to analyse the non-refractory particle species, where non-refractory materials include all species that evaporate in 100 µs under AMS working conditions (Drewnick et al., 2005). In practice, non-refractory material includes species such as ammonium sulfate and bisulfate, ammonium chloride, ammonium nitrate, and organic compounds but excludes black carbon, crustal materials, and sea salt/sodium chloride. Non-refractory species internally mixed with refractory species (e.g., organics internally mixed with black carbon) can be quantitatively detected with the AMS (Katrib et al., 2005; Slowik et al., 2004). The non-refractory particle species that are vaporized at the heated surface (about 600 °C) are then subjected to electron impact ionization, which forms positive ions that are analyzed with a mass spectrometer. The upper 50 % cut-off diameter of the on-board AMS is about 500 nm.

The Ionization Efficiency (IE) calibrations were performed prior and after the campaign as well as five times during the campaign period. The resulting IE showed a good stability and reproducibility (<6 % decrease, caused by detector ageing throughout the campaign). The data shown here are corrected by collection efficiency (CE) factors which were obtained according to (Crosier et al., 2007). All flight data were treated according to procedures provided within the data processing software "Squirrel" and in accordance to the standards defined and currently used by the Aerodyne AMS operators community at the time when these data were treated (http://cires.colorado.edu/jimenez-group/wiki/index.php/Field_Data_Analysis_Guide).

Besides the above mentioned measurements, the ATR-42 was equipped with state-of-the-art aerosol instrumentation: a Particulate Soot Absorption Photometer (PSAP,

ACPD
12, 9451–9490, 2012

Bond et al., 1999), a nephelometer (TSI 3563, TSI Inc., St Paul, MN), particle counting/sizing instruments: a Passive Cavity Aerosol Spectrometer Probe (PCASP-100X). It has to be noted that the filter-based PSAP did not perform accurately during the campaign due to a technical problem. Consequently, PSAP data are not used in this work.

3 Classification of air masses

In order to determine the geographical origins and the history of air masses, retroplume dispersion calculations are performed using the FLEXPART model (version 8.0) that is extensively described in Stohl (1998); Stohl et al. (2005). FLEXPART was driven by 6-hourly ECMWF operational analysis data interleaved with operational forecasts every 3 h (ECMWF, 1995). The model accounts for small-scale turbulence by superimposing stochastic motions on grid-scale winds Stohl and Thomson (1999) and convection using the scheme of Emanuel and Zivkovic-Rothman (1999). FLEXPART was initialized for small segments – corresponding to changes in ATR-42 position or altitude- along the flight track of the ATR-42 and run 20 days backward in time.

FLEXPART results deliver potential emission sensitivity (PES) fields. The PES is based on transport calculations for an inert substance, ignoring removal processes that would reduce the sensitivity. Thus by integrating PES values in the vertical, these fields describe the overall transport of air masses during the 20 days before being sampled by the aircraft. We used the column-integrated PES fields to categorize the sampled air into five sectors of air mass origin. All retroplumes were classified according to their predominent PES values over one of the five sectors before being sampled with the ATR-42 (see Fig. 1). These five sectors have been chosen because of different aerosol sources in these regions.

The following sectors were used for classification of the measurements:

(1) North-West European (NW-EUR) sector corresponding to air masses passing over the Atlantic and the United Kingdom. (2) South-European (S-EUR) sector

ACPD
12, 9451–9490, 2012

corresponding to air masses passing over North Africa, the Atlantic ocean and the Mediterranean or southern Europe. (3) North-East European (NE-EUR) sector corresponding to air masses comming from Scandinavia and passing over the North Sea. (4) East European (E-EUR) sector corresponding to air masses passing over continental Europe. (5) Polar (P) sector corresponding to air masses originating from polar region with expected low particles content.

The meteorological parameters averaged over all 12 flights performed during the campaign, for the five air mass sectors, are given in Table 1. The relative frequency (in percent) the air masses originated from a specific air sector are also reported in Table 1.

A recent study (Hamburger et al., 2010) highlights a strong relationship between the meteorological conditions and the aerosol properties during the whole Longrex (LONG Range EXperiment) project of the EUCAARI campaign. An anticyclonic blocking event occurred during the first half of May 2008 and led to accumulation of particulate pollutants within the boundary layer, while the cyclonic conditions during the second half of the month produced precipitation and led to a cleansing of the atmosphere. Thus, anticyclonic (HP) and cyclonic (LP) conditions will be distinguished in this study (Table 1). The atmospheric pressure at mean sea level, given by air traffic control at the beginning of each flight, has been used to distinguish these two meteorological conditions. In addition, during each flight, one or two vertical soundings were performed at the beginning and/or at the end of the flight, allowing for a charactarization of the vertical evolution of the thermodynamical and microphysical parameters. From these soundings, the inversion level, corresponding to the top of the boundary layer (BL) and the bottom of the free troposphere (FT), determined the mixing layer height, H. Generally, H was > 2000 m during the first half of the month (anticyclonic period) and H < 2000 m during the second half of the month (cyclonic period).

During anticyclonic conditions, air masses were originating from E-EUR (BL, FT), NW-EUR (in the BL only) and NE-EUR (in the FT only). In contrast during cyclonic conditions, air masses were originating from E-EUR, P, S-EUR and NE-EUR (respectively

ACPD
12, 9451–9490, 2012

BL, FT). Thus, air masses sampled by the ATR-42 instrumentation in both layers were more frequently coming from E-EUR during anticyclonic conditions. During cyclonic conditions, NE-EUR were more frequently observed in the BL and S-EUR air masses andwere more frequently observed in the FT.

In the boundary layer, the potential temperatures of S-EUR air masses (<62 K) were significantly lower compared to other air masses. Moreover, the averaged relative humidity (RH) values were beyond 60 %, in the BL, except when air masses were coming from E-EUR (<45 %). On the contrary, these air masses observed in the FT were associated with the highest values of RH (>43 %).

4 Results and discussion

The results indicates that the elevated aerosol loading of investigated air masses occured predominantly in the regions of the Ukraine, Poland and the Northern part of Germany.

4.1 Aerosol concentration

Median values of particle number concentration for the size classes N_{3-10}, N_{10}, N_{50} and N_{500} (i.e. particles with diameter between 3 and 10 nm and larger than 10, 50, and 500 nm, respectively) are given in Table 2. In Figure 2, N_{10} concentration are presented and separated according to cyclonic and anticyclonic conditions and according to the origin of the air mass, in the BL and FT. A large difference in CN concentration can be observed in Fig. 2 and in Table 2. The total aerosol concentrations (N_{10}) are between 1300 and 7090 cm^{-3} within the BL and between 400 and 930 cm^{-3} within the FT. These results are consistent with other airborne measurement studies (Hamburger et al., 2010; Mirme et al., 2010). As the sources of primary particles are mostly located in the BL and air exchange between BL and FT is rather limited, concentrations of particles are higher in the BL compared to the FT.

ACPD
12, 9451–9490, 2012

N_{10} concentrations are more variable in the BL (especially for air masses coming from E-EUR sector during LP conditions) mainly due to the spatial heterogeneities of particle sources. In the FT, the presence of aerosol particles is linked to long range transport, thus, N_{10} concentrations are less variable. However, the variability of the N_{10} concentrations measured in the FT for E-EUR sector during HP conditions is large compare to other air mass sectors. This may be due to variabilities of the meteorological conditions (wind speed, cloud presence, etc.) and of the sector the air mass is originating from (i.e. E-EUR with a relative frequency of 96 %). Differences between BL and FT observations are particularly related to life times of particles in these layers. Indeed, in the boundary layer, particles are freshly emitted while in the FT, particle properties tend to be homogenised during long range transport via cloud processing, coagulation, and sedimentation, etc. (Raes et al., 2000; Williams et al., 2002).

The air mass sectors which are supposed to be the more polluted ones are E-EUR and S-EUR due to the residence of air masses over important industrial areas in Poland, Northern Germany, Spain and France. As expected the median N_{10} concentrations in these two air mass sectors are higher compared to those in the other air mass sectors except in the BL during cyclonic conditions. Indeed, the N_{10} concentrations associated to the cleanest air mass sectors (P and NE-EUR) are surprisingly high in the BL during cyclonic conditions. In fact, these high values are caused by numerous ultra fine particles (N_{3-10}) which reaches 5400 cm^{-3} in P air masses and 3200 cm^{-3} in NE-EUR air masses while the N_{50} are low (1390 and 2900 cm^{-3}, see Table 2).

4.2 Aerosol size distribution

Average particle number size distributions obtained from the SMPS are shown in Figure 3. In general, these number size distributions have been averaged according to air mass origins and subsequently fitted with 3 modal log-normal distributions. Table 3 presents the characteristics of the lognormally fitted size distributions. During the whole campaign, measured distributions (Fig. 3) are generally trimodal in the BL, composed of a nucleation mode $D_{Nucl} < 30$ nm, an Aitken mode ($30 < D_{Aitken} < 60$ nm)

ACPD
12, 9451–9490, 2012

and an accumulation mode ($100 < D_{Acc} < 175$ nm), and bimodal in the FT, composed of an Aitken and an accumulation mode. The nucleation mode, only observed in the boundary layer (Fig. 3a), is centered between 22 and 28 nm during anticyclonic conditions (Fig. 3c) as well as during cyclonic conditions (Fig. 3d). The concentrations of these nucleation modes particles are high (>3000 cm^{-3}) in clean air masses (NEEUR and P), very low (<200 cm^{-3}) in NW-EUR air masses and intermediate (around 1000 cm^{-3}) in polluted air masses (E-EUR and S-EUR).

The Aitken mode is observed either in clean and polluted air masses in the BL as well as in the FT. In the BL, the log normal characteristics of the Aitken mode are similar: the median diameters are between 33.5 and 59.5 nm, the standard deviation ranges between 1.35 and 1.48 and the concentrations are between 327 and 1975 cm^{-3}. In the FT, the mean diameter of the Aitken mode (between 35.8 and 55.3 nm) are similar to those observed in the BL.

The large difference found for N_{10} concentration, between BL and FT levels, is also observed for the concentrations of accumulation mode particles. Indeed, these concentrations are higher than 1200 cm^{-3} in the BL (except for NW-EUR air masses) comparable with ground site observations reported in Hamburger et al. (2010) and lower than 850 cm^{-3} in the FT.

A comparison of the median diameter observed during both meteorological conditions highlights that the median diameter of the accumulation mode is larger in the free troposphere during anticyclonic conditions, by a factor between 1.1 and 1.7. These changes are quantitatively consistent with (Hamburger et al., 2010). Moreover,in two air masses under cyclonic conditions (E-EUR in the BL and P in the FT), the size distributions could be represented by only one broad ($\sigma >= 1.8$) accumulation mode (95–128 nm). These observations indicates that that particles have resided a longer time in the atmosphere during which they have grown by coagulation, merging of two modes, condensation of gases and interactions with clouds.

For each size distribution presented in Fig. 3, the total volume concentration was calculated by integrating the size spectrum, assuming a spherical shape for the particles.

ACPD
12, 9451–9490, 2012

These total volume concentrations are reported in Table 4 with the volume concentration of refractory particles similarly calculated from the heated SMPS. Significant differences in the calculated volume concentrations are observed for the different air mass sectors. E-EUR and S-EUR air masses passing over industrial and densely populated areas have the highest aeosol loadings (>9.59 $\mu m^3\,cm^{-3}$ in the BL and >3.48 $\mu m^3\,cm^{-3}$ in the FT). Interestingly, low aerosol loadings are associated with air masses passing over United Kingdom in the BL (NW-EUR : 0.71 $\mu m^3\,cm^{-3}$). In the FT, clean air was observed in NE-EUR (lowest volume concentrations <0.46 $\mu m^3\,cm^{-3}$) consistent with previous results of Van Dingenen et al. (2005). The fraction of refractory matter, given by the ratio of the refractory volume over total volume of sampled particles (Table 4), is higher in the FT than in the BL during cyclonic conditions. These latter results should be related to larger concentrations of condensable gases close to the different sources present in the BL versus the presence of more refractory particles (dust or sea salt particles) from long range transport in the FT.

4.3 Aerosol chemical composition and mass concentration

The average relative concentrations for organic, nitrate, sulfate, ammonium and chloride measured by the AMS are given in Fig. 4 as a function of the air mass origin. Mass concentrations of non-refractory submicron particles corresponding to the sum of all these components are plotted in Fig. 5. The mass concentration of refractory material is estimated by using the size distribution of particles ($Dp < 500$ nm) sampled downstream a thermo-desorption column (V-SMPS), by assuming that refractory particles are spherical and by using a density of 1.8 $g\,cm^{-3}$ determined by Slowik et al. (2007). The mass concentration of refractory and non-refractory material are then added and plotted in Fig. 5.

In the BL, two different groups of air mass sectors can be distinguished according to the particle chemical composition independently of the synoptic conditions: Group I (E-EUR and S-EUR) and Group II (NW-EUR and NE-EUR). For the Group II, we observe high nitrate concentrations (>5 $\mu g\,m^{-3}$) and the chloride concentrations reaching

ACPD
12, 9451–9490, 2012

0.61 and 0.25 $\mu g\,m^{-3}$ for 0.61 and 0.25 $\mu g\,m^{-3}$ for NW-EUR and NE-EUR, respectively. associate with an increase in chloride concentration may originate from natural (marine aerosol) or anthropogenic sources (industry exhaust). The refractory material concentration is six times higher during NE-EUR periods (1.48 $\mu g\,m^{-3}$) than during NW-EUR periods (0.24 $\mu g\,m^{-3}$). (1.48 $\mu g\,m^{-3}$) than during NW-EUR periods (0.24 $\mu g\,m^{-3}$). Obviously, this reflects the fact that the NE-EUR sector is more influenced by anthropogenic aerosol contributions, while marine aerosol contributions are much more important during NW-EUR periods. The aerosol relative and absolute chemical compositions of Group I is similar to the one observed in or around a highly polluted urban area (Mexico city) during the Milagro airborne campaign (DeCarlo et al., 2008). Organics are the major component (about 50 %) and nitrates are the second most important component (20 %). Sulfate and ammonium relative concentrations are about

In the BL, air masses originating from S-EUR sector have the highest mass concentration (29 $\mu g\,m^{-3}$) and the highest refractory material material level (5.24 $\mu g\,m^{-3}$) consistent with the highest aerosol volume concentrations in the polluted air masses. In particular, the absolute concentrations of organics reach 18 $\mu g\,m^{-3}$ corresponding to values generally observed in different urban areas like (Zhang et al., 2005), Mexico City (Volkamer et al., 2006) or Zurich (Lanz et al., 2007). The NW-EUR air masses were found to be much cleaner according to the volume concentration and the refractory material level (0.24 $\mu g\,m^{-3}$). However, the total mass concentration (16 $\mu g\,m^{-3}$) is still high and corresponds to roughly 50 % of the upper value.

In the FT, the air mass characteristics highlighted by the volume concentration are consistent with those given by the total mass concentration. Indeed, the highest values of the mass concentration are associated with E-EUR air masses while the lowest are associated with NE-EUR air masses while the S-EUR air masses are enriched in refractory material (2.01 $\mu g\,m^{-3}$). A clear signature can be seen for the chemical composition of particles originating from NE-EUR during anticyclonic conditions. Indeed, the predominant chemical components of 90 % of the measured mass concentration of non refractory aerosol are sulfate and ammonium. The remaining 10 % mass concentration

ACPD
12, 9451–9490, 2012

measured by the AMS is composed mainly of nitrate and organics. Moreover, the organic absolute fractions for NE-EUR are low (>0.05 $\mu g\,m^{-3}$) which is comparable to results of a study on background rural aerosol particles (Hock et al., 2008). This particular chemical composition might be linked to the presence of high concentrations of condensable inorganic gases, i.e. dimethylsulphide or H_2SO_4, over the sea. In situ measurements performed at coastal sites Rinaldi et al. (2009); Asmi et al. (2010) highlight that the major components (>60 %) of aerosol particles with diameter smaller than 800 nm are sulfate and ammonium. These observations in the BL seems to be comparable to the EUCAARI results in the FT. Thus, the comparison of these results might show a strong relationship between the BL and the FT, but as no measurements of NE-EUR were performed in the BL during anticyclonic conditions, this cannot be proven.

The comparison between BL and FT measurements reveals different behaviour as a function of the synoptic conditions. During cyclonic conditions in the FT, the nitrate contribution decreases significantly by a factor of 0.6 while the sulfate fraction increases by a factor of 1.5, for Group I air mass (E-EUR and W-EUR).

The relative fraction of refractory material in the aerosol composition has been calculated for polluted air masses (E-EUR and S-EUR) as well as for clean air masses (others) in both layers. The average refractory material fraction is about 5.5 % for clean air masses and 13.8 % for polluted air masses in the BL, while, in the FT, this fraction is high (between 10.8 % and 61.8 %) for clean air masses and similar (13.2 %) to those observed in the BL for polluted air masses. FLEXPART simulations point towards many biomass burning events only during clean air mass periods which might lead to this unusualy large fraction of refractory material. The refractory material similarities between both layers in polluted air masses is probably due to fast occasional mixing of both layers. Recent studies (Venzac et al., 2008, 2009) show that mixing between both layers may be enhanced through the residual layer.

ACPD
12, 9451–9490, 2012

4.4 CCN properties

To characterize the relationship between cloud condensation nuclei (CCN) and corresponding aerosol populations, the CCN/CN ratio can be introduced as a measure of hygroscopicity of the aerosol population. However, since measurements made with both CPCs include numerous ultra-fine particles which are not likely to act as CCN, the total CN concentration cannot be used as a reference for the aerosol concentration. Thus, taking into account an average value of 50 nm as the minimum activation diameter for aerosol particles of continental origin, SMPS measurements were used to provide the N_{50} concentration required to calculate a CCN/N_{50} ratio. The evolution of the CCN/N_{50} ratio as a function of air mass groups sampled during EUCAARI is shown in Figure 6. As this ratio is highly dependent on the aerosol concentrations, also the CCN number concentrations have been plotted (black points) for all air mass groups. During the anticyclonic conditions, no CCN data have been acquired in the NE-EUR sector air masses.

In the BL, the values of the CCN/N_{50} ratios (0.17-0.22) are similar for all air mass groups and for both cyclonic and anticyclonic conditions while the CCN concentrations range from very low values (<70 cm^{-3}, for NW-EUR sector) to high values (1570 cm^{-3} for W-EUR sector). The lowest values of the CCN/N_{50} ratio are associated with aerosol originating from marine sources while higher values are associated with higher concentrations of larger particles (Fig. 3). Despite the CCN/N_{50} ratio is rather constant (around 0.2) consistent with the same chemical composition of particles. Thus we can assume that particle size and/or atmospheric dynamics is not playing a major role in this case. The measurement variability, i.e. 120 %, is similar for all air mass groups except in NW-EUR air masses, in which it is higher, likely because of very low CCN and N_{50} concentrations.

In the FT, the CCN concentrations (65–420 cm^{-3}) at most three times lower than values observed in the BL and the N_{50} concentrations are at least three times lower than in the BL concentrations. Hence, the CCN/N_{50} ratio is higher in the FT (0.19–0.44)

ACPD
12, 9451–9490, 2012

than in the BL. Because the number size distribution of aerosol particles do not show a smaller fraction of particles in the activation range (50–100 nm) in the FT compared to the BL, higher CCN/N_{50} in the FT can be partly related to the chemical composition of aerosol particles showing a significant increase in relative and absolute concentrations of soluble material in the FT as compared to the BL. The alteration of particles surface properties by a coating formed during their transport (Clarke et al., 2004; Zhang et al., 2005; Ekman et al., 2006; Matsuki et al., 2010) may explain this increase of solubility.

One can note that, in the BL as well as in the FT, the highest CCN concentrations are measured for the most polluted sectors (E-EUR and S-EUR, Fig. 6) while the highest CCN/N_{50} ratio values are measured for polar air masses in the FT.

4.5 Optical properties

Figure 7 presents the ratio of the total scattering coefficient measured by the nephelometer to the number concentration of optically active particles with diameter larger than 150 nm. This normalised ratio corresponds to the average scattering efficiency of one optically active particle, i.e. the particle scattering cross-section. A few measurements with very low values of the scattering coefficient ($<5 M m^{-1}$), mainly found for two different air mass sectors (NE-EUR and NW-EUR), have been removed, since the scattering cross-section cannot be safely derived for these data. During anticyclonic conditions, only observations from E-EUR are presented, both in the BL and in the FT. The average scattering cross-section of a particle is about $0.026\,\mu m^{-2}$ in the BL and $0.052\,\mu m^{-2}$ in the FT. Thus, particles sampled in the FT scatter light two times more efficiently than particles sampled in the BL.

During cyclonic situations, the average scattering cross-section is lower than $0.064\,\mu m^{-2}$ in the BL. The maximum value is associated with polar air masses while minimum values (about $0.032\,\mu m^{-2}$) are calculated for NE-EUR and E-EUR sectors. It is interesting to note that aerosol particles from the more (E-EUR) and the less (NE-EUR) polluted air masses have the same scattering efficiency.

ACPD
12, 9451–9490, 2012

In the free troposphere, the average values of the scattering cross section is larger than $0.04\,\mu m^{-2}$ but the general trend, according to the different air masses, is totally the opposite of the one observed in the boundary layer. Indeed, the average scattering cross-section of aerosol particles from polar air masses is the weakest ($0.048\,\mu m^{-2}$) while for polluted air masses (E-EUR and S-EUR) values are higher (around $0.13\,\mu m^{-2}$). When comparing values observed in the BL and in the FT during cyclonic conditions, one can conclude that the scattering cross-sections of particles are 4 times higher in the FT than in the BL for the polluted air masses (E-EUR, W-EUR), while they are 1.33 time higher in the BL than in the FT for polar air masses. As the optical impact of aerosol particles are dependant on the surface properties, these considerable differences between both layers are probably a consequence of different coating. Indeed, the presence of aerosol particles in the FT is connected to long range transport leading to the presence of more or less complete coating on the aerosol particle surface (Falkovich et al., 2004; Zhang et al., 2005; Ekman et al., 2006; Roger, 2009; Matsuki et al., 2010). In contrast, aerosol particles in the BL have had less time to be altered since emission (Doran et al., 2007).

To complete this set of optical parameters, the scattering Angström exponent (Kim et al., 2004) as well as the scattering asymmetry factor (Sagan and Pollack, 1967) have been calculated. The Angström exponent is determined from the spectral dependance measured by the nephelometer between two wavelengths (450 nm and 650 nm). The Angström exponent is often used as a qualitative indicator of aerosol particle size, with values greater than 2 indicating small particles associated with combustion byproducts, and values less than 1 indicating large particles like sea salt and dust (Dubovik et al., 2002; Kim et al., 2004). The asymmetry parameter, g, is a numerical value related to the difference between forward-scattered and backward-scattered electromagnetic radiation in the atmosphere. Because of the computational inefficiency of using exact scattering phase functions, g is often used to parameterize the phase function in the two-stream radiation transfer approximation.

ACPD
12, 9451–9490, 2012

For air masses with large scattering coefficient values (>5 M m^{-1}), the average asymmetry factor values are between 0.60 and 0.80. This parameter is thus not relevant to distinguish between different air masses (Coming soon ref from JC Roger). However, plotted as a function of the scattering Angström exponent (Fig. 8), some tendencies can be pointed out. Indeed, the scatterplot in Figure 8 shows two domains, one corresponding to low Angström exponents (<0.35) and thus larger particles, and the second one to higher Angström exponents (>0.45) related to finer particles. Both cases occur in the FT while only cases with high Angström exponent are observed in the BL. The majority of particles observed in the FT, associated with low Angström exponents, are large particles which is consistent with long range transport processing. The majority of particles observed in the FT, associated with low Angström exponents, are large particles which is consistent with long range transport processing and with dust plume originating from North Africa. Moreover, the high negative values of the Angström exponent is found to be related to 'frozen' particles which are spectrally white. Indeed, the total liquid water is found to be maximum and the temperature is found to be the minimum when the Angström exponent values are negative. The large Angström exponent value are associated with fine particles which is consistent with the proximity to emission sources. Some of the particles sampled in the FT have similar optical properties as particles sampled in the BL, probably due to fast exchange between both layers as suggested earlier.

5 Conclusions

A comprehensive set of instruments performing meteorological, cloud microphysics and aerosol physico-chemical and optical measurements was integrated on the French research aircraft ATR-42 for the EUCAARI intensive observation period. The measurements obtained document clear relations between aerosol properties and air mass origins. Based on backward calculations with a Lagrangian particle dispersion model, the observed air masses were classified into five sectors according to their predominent

ACPD
12, 9451–9490, 2012

residence times in these sectors. Moreover, measurements performed under anticyclonic (during first half of the campaign duration) and cyclonic (during second half of the campaign duration) synoptic conditions were distinguished and analyzed separately.

The observations reveal a strong difference of N_{50} particle number concentrations between the boundary layer (BL) and the free troposphere (FT). In particular, N_{50} concentration are about five times higher within the BL as compared to those observed within the FT. Observed size distributions are rather trimodal in the BL (nucleation, Aitken and accumulation modes) and generally bimodal in the FT (Aitken and accumulation modes). In the FT, significant refractory material fractions, derived from volatility measurements, were observed during cyclonic conditions. This is probably the consequence of a long-range transport of biomass burning particles and/or the fast mixing of air from the BL into the FT as it has been observed for polluted air mass cases. This fast occasional mixing has been confirmed by the similarities found for aerosol optical properties in both layers.

Polluted air masses are characterised by high total number particle concentrations and low concentrations of fine particles (N_{10-50}). In the BL, the total mass concentration as well as the aerosol chemical composition are similar to those observed in highly polluted areas, like for example in the region around Mexico City DeCarlo et al. (2008). The relative chemical composition of particles within polluted air masses is dominated by organics (about 50 %) and nitrates (20 %) with notable amounts of sulfate.

Non-polluted air masses, in general originating from polar and Scandinavian regions, are characterised by high total particle concentrations most likely due to new particle formation events occurring over the sea. The chemical composition of particles within polar air masses in the BL are characterised by significant amounts of chloride and nitrate species most likely from NH_4Cl probably originating from marine sources, in the BL, and by the strong influence of sulfate and ammonium (>90 % of the AMS components) linked to the presence of high contents of condensable gases over Scandinavia.

The comparison of observations carried out during both synoptic conditions (anticyclonic, cyclonic) highlights an increase of the median diameter of accumulation

ACPD
12, 9451–9490, 2012

particles during anticyclonic conditions consistent with Hamburger et al. (2010). Moreover, differences in chemical properties have been observed as a function of meteorological conditions when comparing measurements in both layers. During cyclonic conditions, the nitrate concentrations are significantly lower and sulfate concentrations increase in the FT compared to chemical composition of particles in the BL. In contrast, during anticyclonic conditions, the sulfate and the ammonium concentrations are relatively higher in the FT compared to those observed in the BL. Finally, during cyclonic conditions, the average values of the scattering cross-section (as well as the particle surface concentrations) for particles in the FT are higher than those in the BL, probably due to the coating of particles during the long range transport.

Acknowledgements. This work has been partially funded by European Commission 6th Framework program project EUCAARI, contract no 036833-2 (EUCAARI), and by the French National Research Agency (ANR) under the AEROCLOUD program, contract no 06-BLAN-0209. Suzanne Crumeyrolle has been supported by CNRS fellowship (contract no. 167641). The authors wish to thank the SAFIRE (Service des Avions Français Instruments pour la Recherche en Environnement) for preparing and delivering the research aircraft (ATR-42).

The publication of this article is financed by CNRS-INSU.

References

Adams, P. J. and Seinfeld, J. H.: Predicting global aerosol size distributions in general circulation models, J. Geophys. Res., 107, 4370, doi:10.1029/2001JD001010, 2002. 9453

ACPD
12, 9451–9490, 2012

Adams, P. J. and Seinfeld, J. H.: Predicting global aerosol size distributions in general 3 circulation models, J. Geophys. Res., 107, 4370, doi:10.1029/2001JD001010, 2002. 9453
Andreae, M. O. and Crutzen, P. J.: Atmospheric Aerosols: Biogeochemical sources and role in atmospheric chemistry, Science, 276, 1052–1058, 1997. 9453
Asmi, E., Frey, A., Virkkula, A., Ehn, M., Manninen, H. E., Timonen, H., Tolonen-Kivimäki, O., Aurela, M., Hillamo, R., and Kulmala, M.: Hygroscopicity and chemical composition of Antarctic sub-micrometre aerosol particles and observations of new particle formation, Atmos. Chem. Phys., 10, 4253–4271, doi:10.5194/acp-10-4253-2010, 2010. 9464
Bauer, S. E. and Koch, D.: Impact of heterogeneous sulfate formation at mineral dust surfaces on aerosol loads and radiative forcing in the Goddard Institute for Space Studies general circulation model, J. Geophys. Res., 110, D17202, doi:10.1029/2005JD005870, 2005.
Bond T. C., Anderson T. L., and Campbell, D.: Calibration and Intercomparison of Filter-Based Measurements of Visible Light Absorption by Aerosols, Aerosol Sci. Tech., 30, 582–600, 1999. 9457
Brenguier, J. L., Bourrianne, T., Coelho, A., Isbert, J., Peytavi, R., Trevarin, D., and Wechsler, P.: Improvements of droplet size distribution measurements with the Fast-FSSP, J. Atmos. Oceanic. Technol., 15, 1077–1090, 1998.
Canagaratna, M. R., Jayne, J. T., Jimenez, J. L., Allan, J. D., Alfarra, M. R., Zhang, Q., Onasch, T. B., Drewnick, F., Coe, H., Middlebrook, A., Delia, A., Williams, L. R., Trimborn, A. M., Northway, M. J., DeCarlo, P. F., Kolb, C. E., Davidovits, P., and Worsnop, D. R.: Chemical and Microphysical Characterization of Ambient Aerosols with the Aerodyne Aerosol Mass Spectrometer, Mass Spectrom. Rev., 26, 185–222, 2007. 9456
Chýlek, P., Lesins, G. B., Videen, G., Wong, J. G. D., Pinnick, R. G., Ngo, D., and Klett, J. D.: Black carbon and absorption of solar radiation by clouds, J. Geophys. Res.-Atmos., 101, 23365–23371, 1996.
Clarke, A. D., Shinozuka, Y., Kapustin, V. N., Howell, S., Huebert, B., Doherty, S., Anderson, T., Covert, D., Anderson, J., Hua, X., Moore, K. G., McNaughton, C., Carmichael, G., and Weber, R.: Size distributions and mixtures of dust and black carbon aerosol in Asian outflow: Physiochemistry and optical properties, J. Geophys. Res., 109, D15S09, doi:10.1029/2003JD004378, 2004. 9466
Crumeyrolle, S., Gomes, L., Tulet, P., Matsuki, A., Schwarzenboeck, A., and Crahan, K.: Increase of the aerosol hygroscopicity by cloud processing in a mesoscale convective

ACPD
12, 9451–9490, 2012

system: a case study from the AMMA campaign, Atmos. Chem. Phys., 8, 6907–6924, doi:10.5194/acp-8-6907-2008, 2008. 9454

Crumeyrolle, S., Manninen, H. E., Sellegri, K., Roberts, G., Gomes, L., Kulmala, M., Weigel, R., Laj, P., and Schwarzenboeck, A.: New particle formation events measured on board the ATR-42 aircraft during the EUCAARI campaign, Atmos. Chem. Phys., 10, 6721–6735, doi:10.5194/acp-10-6721-2010, 2010. 9454

Crumeyrolle, S., Weigel, R., Sellegri, K., Roberts, G., Gomes, L., Stohl, A., Laj, P., Bourianne, T., Etcheberry, J. M., Villani, P., Pichon, J. M., Schwarzenboeck, A.: Impact of cloud processing on the phase partitioning of aerosol particles: results from two ATR-42 flights in an extended stratocumulus cloud layer during the EUCAARI campaign (2008), in preparation, 2011.

Crosier, J., Allan, J. D., Coe, H., Bower, K. N., Formenti, P., and Williams P. I.: Chemical Composition of Summertime Aerosol in the Po Valley (Italy), Northern Adriatic and Black Sea, Q. J. Roy. Meteor. Soc., 133, 61–75, doi:10.1002/qj.88, 2007. 9456

DeCarlo, P. F., Dunlea, E. J., Kimmel, J. R., Aiken, A. C., Sueper, D., Crounse, J., Wennberg, P. O., Emmons, L., Shinozuka, Y., Clarke, A., Zhou, J., Tomlinson, J., Collins, D. R., Knapp, D., Weinheimer, A. J., Montzka, D. D., Campos, T., and Jimenez, J. L.: Fast airborne aerosol size and chemistry measurements above Mexico City and Central Mexico during the MILAGRO campaign, Atmos. Chem. Phys., 8, 4027–4048, doi:10.5194/acp-8-4027-2008, 2008. 9463, 9469

Doran, J. C., Barnard, J. C., Arnott, W. P., Cary, R., Coulter, R., Fast, J. D., Kassianov, E. I., Kleinman, L., Laulainen, N. S., Martin, T., Paredes-Miranda, G., Pekour, M. S., Shaw, W. J., Smith, D. F., Springston, S. R., and Yu, X.-Y.: The T1–T2 study: evolution of aerosol properties downwind of Mexico City, Atmos. Chem. Phys., 7, 1585–1598, doi:10.5194/acp-7-1585-2007, 2007. 9467

Drewnick, F., Hings, S. S., DeCarlo, P. F., Jayne, J. T., Gonin M., Fuhrer, K., Weimer, S., Jimenez, J. L., Demerjian, K. L., Borrmann, S., Worsnop, D. R.: A new Time-of-Flight Aerosol Mass Spectrometer (ToF-AMS) Instrument Description and First Field Deployment, Aerosol Sci. Tech., 39, 637–658, 2005. 9456

Dubovik, O., Holben, B. N., Eck, T. F., Smirnov, A., Kaufman, Y. J., King, M. D., Tanre, D., and Slutsker, I.: Variability of absorption and optical properties of key aerosol types observed in worldwide locations, J. Atmos. Sci., 59, 590–608, 2002. 9467

ECMWF: User Guide to ECMWF Products 2.1, Meteorol. Bull. M3.2, ECMWF, Reading, UK, 1995. 9457

ACPD

12, 9451–9490, 2012

Ekman, A. M. L., Wang, C., Wilson, J., Ström, J., and Krejci, R.: Explicit Simulation of Aerosol Physics in a Cloud-Resolving Model: Aerosol Transport and Processing in the Free Troposphere, J. Atmos. Sci., 63, 682–696, 2006. 9466, 9467

Emanuel, K. A. and Zivkovic-Rothman, M.: Development and evaluation of a convection scheme for use in climate models, J. Atmos. Sci., 56, 1766–1782, 1999. 9457

Falkovich, A. H., Schkolnik, G., Ganor, E., and Rudich, Y.: Adsorption of organic compounds pertinent to urban environments onto mineral dust particles, J. Geophys. Res.-Atmos., 109, D01201, doi:01210.01029/02003JD003919, 2004. 9467

Guazzotti, S. A., Whiteaker, J. R., Suess, D., Coffee, K. R., and Prather, K. A.: Real-time measurements of the chemical composition of size-resolved particles during a Santa Ana wind episode, California USA, Atmos. Environ., 35, 3229–3240, 2001.

Hamburger, T., McMeeking, G., Minikin, A., Birmili, W., Dall'Osto, M., O'Dowd, C., Flentje, H., Henzing, B., Junninen, H., Kristensson, A., de Leeuw, G., Stohl, A., Burkhart, J. F., Coe, H., Krejci, R., and Petzold, A.: Overview of the synoptic and pollution situation over Europe during the EUCAARI-LONGREX field campaign, Atmos. Chem. Phys., 11, 1065–1082, doi:10.5194/acp-11-1065-2011, 2011. 9458, 9459, 9461, 9470

Haywood, J., Francis, P., Osborne, S., Glew, M., Loeb, N., Highwood, E., Tanre, D., Myhre, G., Formenti, P., and Hirst, E.: Radiative properties and direct radiative effect of Saharan dust measured by the C-130 aircraft during SHADE: 1. Solar spectrum, J. Geophys. Res., 108, 8577, doi:10.1029/2002JD002687, 2003. 9453

Hock, N., Schneider, J., Borrmann, S., Römpp, A., Moortgat, G., Franze, T., Schauer, C., Pöschl, U., Plass-Dülmer, C., and Berresheim, H.: Rural continental aerosol properties and processes observed during the Hohenpeissenberg Aerosol Characterization Experiment (HAZE2002), Atmos. Chem. Phys. Discuss., 7, 8617–8662, doi:10.5194/acpd-7-8617-2007, 2007. 9464

IPCC: Intergovernmental Panel on Climate Change. Climate Change 2007, The Physical Science Basis: Contribution of Working Group I to the Fourth Assessment Report of the IPCC, Cambridge: Cambridge University Press, 2007. 9453

Jayne J. T., Leard, D. C., Zhang, X., Davidovits, P., Smith, K. A., Kolb, C. E., and Worsnop, D. R.: Development of an Aerosol Mass Spectrometer for Size and Composition Analysis of Submicron Particles, Aerosol Sci. Tech., 33, 49–70, 2000.

Jokinen, V. and Mäkelä, J.: Closed loop arrangement with critical orifice for DMA sheath/excess fl ow system, J. Aerosol Sci., 28, 643–648, 1996.

ACPD
12, 9451–9490, 2012

Kaufman, Y. J., Tanre, D., and Boucher, O.: A satellite view of aerosols in the climate system, Nature, 419, 215–223, 2002. 9455
9453
Katrib, Y., Martin, S. T., Rudich, Y., Davidovits, P., Jayne, J. T., and Worsnop, D. R.: Density changes of aerosol particles as a result of chemical reaction, Atmos. Chem. Phys., 5, 275–291, doi:10.5194/acp-5-275-2005, 2005. 9456
Kaufman, Y. J., Tanre, D., and Boucher, O.: A satellite view of aerosols in the climate system, Nature, 419, 215–223, 2002. 9453
Kim, D.-H., Sohn, B.-J., Nakajima, T., Takamura, T., Takemura, T., Choi, B.-C., and Yoon, S.-C.: Aerosol optical properties over east Asia determined from ground-based sky radiation measurements, J. Geophys. Res., 109, D02209, doi:10.1029/2003JD003387, 2004. 9467
Korolev, A. V., Nevzorov, A. N., Strapp, J. W., and Isaac, G. A.: The Nevzorov Airborne Hot-Wire LWC-TWC Probe : Principle of Operation and Performance Characteristics, J. Atmos. Ocean.Tech., 15, 1495–1510, 1998.
Kulmala, M., Asmi, A., Lappalainen, H. K., Carslaw, K. S., Pöschl, U., Baltensperger, U., Hov, Ø., Brenquier, J.-L., Pandis, S. N., Facchini, M. C., Hansson, H.-C., Wiedensohler, A., and O'Dowd, C. D.: Introduction: European Integrated Project on Aerosol Cloud Climate and Air Quality interactions (EUCAARI) – integrating aerosol research from nano to global scales, Atmos. Chem. Phys., 9, 2825–2841, doi:10.5194/acp-9-2825-2009, 2009. 9453
Lanz, V. A., Alfarra, M. R., Baltensperger, U., Buchmann, B., Hueglin, C., and Prévôt, A. S. H.: Source apportionment of submicron organic aerosols at an urban site by factor analytical modelling of aerosol mass spectra, Atmos. Chem. Phys., 7, 1503–1522, doi:10.5194/acp-7-1503-2007, 2007. 9463
Lesins, G., Chýlek, P., and Lohmann, U.: A study of internal and external mixing scenarios and its effect on aerosol optical properties and direct radiative forcing, J. Geophys. Res.-Atmos., 107, 4094, doi:4010.1029/2001JD000973, 2002.
Lohmann, U., Broekhuizen, K., Leaitch, R., Shantz, N., and Abbatt, J.: How efficient is cloud droplet formation of organic aerosols?, Geophys. Res. Lett., 31, L05108, doi:10.1029/2003GL018999, 2004. 9453
Matsuki, A., Schwarzenboeck, A., Venzac, H., Laj, P., Crumeyrolle, S., and Gomes, L.: Cloud processing of mineral dust: direct comparison of cloud residual and clear sky particles during AMMA aircraft campaign in summer 2006, Atmos. Chem. Phys., 10, 1057–1069, 2010, http://www.atmos-chem-phys.net/10/1057/2010/. 9454, 9466, 9467

ACPD
12, 9451–9490, 2012

McMurry, P. H.: The History of CPCs, Aerosol Sci. Technol., 33, 297–322, 2000. 9455
McNaughton, C. S., Clarke, A. D., Howell, S. G., Pinkerton, M., Anderson, B., Thornhill, L., Hudgins, C., Winstead, E., Dibb, J. E., Sceuer, E., and Maring, H.: Results from the DC-8 Inlet Characterization Experiment (DICE): Airborne Versus Surface Sampling of Mineral Dust and Sea Salt Aerosols, Aerosol Sci. Technol., 41, 136–159, 2007. 9455
Mertes, S., Schrooder, F., and Wiedensohler, A.: The particle detection efficiency curve of the TSI3010 CPC as a function of temperature difference between saturator and condenser, Aerosol Sci. Tech., 23, 257–270, 1995. 9455
Meskhidze, N., Remer, L. A., Platnick, S., Negrón Juárez, R., Lichtenberger, A. M., and Aiyyer, A. R.: Exploring the differences in cloud properties observed by the Terra and Aqua MODIS Sensors, Atmos. Chem. Phys., 9, 3461–3475, doi:10.5194/acp-9-3461-2009, 2009.
Mirme, S., Mirme, A., Minikin, A., Petzold, A., Hõrrak, U., Kerminen, V.-M., and Kulmala, M.: Atmospheric sub-3 nm particles at high altitudes, Atmos. Chem. Phys., 10, 437–451, doi:10.5194/acp-10-437-2010, 2010. 9459
Nafstad, P., Haheim, L. L., Oftedal, B., Gram, F., Holme, I., Hjermann, I., and Leren, P.: Lung cancer and air pollution: a 27 years follow-up of 16 209 Norwegian men, Thorax 58, 1071–1076, 2003.
Parungo, F., Kopcewicz, B., Nagamoto, C., Schnell, R., Sheridan, P., Zhu, C., and Harris, J.: Aerosol Particles in the Kuwait Oil Fire Plumes: Their Morphology, Size Distribution, Chemical Composition, Transport, and Potential Effect on Climate, J. Geophys. Res., 97(D14), 15, 867–882, 1992.
Philippin, S., Laj, P., Putaud J.-P., Wiedensohler, A., de Leeuw, G., Fjaeraa, A. M., Platt, U., Baltensperger, U., and Fiebig, M.: EUSAAR – An Unprecedented Network of Aerosol Observation in Europe, Earozoru Kenkyu, JAAST, 24(2), 78–83, 2009.
Pope, C. A., Burnett, R. T., Thun, M. J., Calle, E. E., Krewski, D., Ito, K., and Thurston, G. D.: Lung cancer, cardiopulmonary mortality and long term exposure to fine particulate air pollution, JAMA, 287, 1132–1141, 2002.
Pope, C. A. and Dockery, D. W.: Health effects of fine particulate air pollution: lines that connect, 30, J. Air Waste Manage., 56, 709–742, 2006.
Raes, F., van Dingenen, R., Vignati, E., Wilson, J., Putaud, J.-P., Seinfeld, J. H., and Adams, P.: Formation and cycling of aerosols in the global troposphere, Atmos. Environ., 34, 4215–4240, 2000. 9460

ACPD
12, 9451–9490, 2012

Res, J. G., Schwarz, J. P., Gao, R. S., Fahey, D. W., Thomson, D. S., Watts, L. A., Wilson, J. C., Reeves, J. M., Darbeheshti, M., Baumgardner, D. G., Kok, G. L., Chung, S. H., Schulz, M., Hendricks, J., Lauer, A., Karcher, B., Slowik, J. G., Rosenlof, K. H., Thompson, T. L., Langford, A. O., Loewenstein, M., and Aikin, K. C.: Single-particle measurements of midlatitude black carbon and light-scattering aerosols from the boundary layer to the lower stratosphere, J. Geophys. Res.-Atmos., 111, D16207, doi:10.1029/2006JD007076, 2006.

Roberts, G. C. and Nenes, A.: A Continuous-Flow Streamwise Thermal-Gradient CCN Chamber for Atmospheric Measurements, Aerosol Sci. Technol., 39, 206–221, 2005. 9455

Roberts, G. C., Andreae, M. O., Zhou, J., and Artaxo, P.: Cloud condensation nuclei in the Amazon Basin: Marine conditions over a continent?, Geophys. Res. Lett., 28, 2807–2810, 2001. 9453

Roger, J. C., Guinot, B., Cachier, H., Mallet, M., Dubovik, O., and Yu, T.: Aerosol complexity in megacities: From size resolved chemical composition to optical properties of the Beijing atmospheric particles, Geophys. Res. Lett., 36, L18806, doi:10.1029/2009GL039238, 2009. 9467

Rinaldi, M., Facchini, M. C., Decesari, S., Carbone, C., Finessi, E., Mircea, M., Fuzzi, S., Ceburnis, D., Ehn, M., Kulmala, M., de Leeuw, G., and O'Dowd, C. D.: On the representativeness of coastal aerosol studies to open ocean studies: Mace Head a case study, Atmos. Chem. Phys., 9, 9635–9646, doi:10.5194/acp-9-9635-2009, 2009. 9464

Sagan, C. and Pollack, J. B.: Anisotropic nonconservative scattering and the clouds of Venus, J. Geophys. Res., 72, 469–477, 1967. 9467

Schwarzenboeck A., and Heintzenberg J., and M. Mertes. Incorporation of aerosol particles between 25 and 850 nm into cloud elements: measurements with a new complementary sampling system, Atmos. Res., 52, 241–260, 2000.

Slowik, J. G., Stainken, K., Davidovits, P., Williams, L. R., Jayne, J. T., Kolb, C. E., Worsnop, D. R., Rudich, Y., DeCarlo, P., and Jimenez, J. L.: Particle Morphology and Density Characterization by Combined Mobility and Aerodynamic Diameter Measurements. Part 2: Application to combustion Generated Soot Aerosols as a Function of Fuel Equivalence Ratio, Aerosol Sci. Technol., 38, 1206–1222, 2004. 9456

Slowik J. G., Cross, E. S., Han, J., Davidovits, P., Onasch, T. B., Jayne, J. T., Williams, L. R., Canagaratna, M. R., Worsnop, D. R., Chakrabarty, R. K., Moosmüller, H., Arnott, W. P., Schwarz, J. P., Gao, R., Fahey, D. W., Kok, G. L., and Petzold, A.: An Inter-Comparison

ACPD
12, 9451–9490, 2012

of Instruments Measuring Black Carbon Content of Soot Particles, Aerosol Sci. Tech., 41, 295–314, 2007. 9462
Song, C. H. and Carmichael, G. R.: The aging process of naturally emitted aerosol (sea10 salt and mineral aerosol) during long range transport, Atmos. Environ., 33, 2203–2218, 1999.
Spichtinger, P. and Cziczo, D. J.: Aerosol cloud interactions a challenge for measurements and modeling at the cutting edge of cloud–climate interactions, Environ. Res. Lett., 3, 025002, doi:10.1088/1748-9326/3/2/025002, 2008. 9453
Stohl, A., Hittenberger, M., and Wotawa, G.: Validation of the Lagrangian particle dispersion model FLEXPART against large scale tracer experiment data, Atmos. Environ., 24, 4245–4264, 1998. 9457
Stohl, A. and Thomson, D. J.: A density correction for Lagrangian particle dispersion models, Bound.-Lay. Meteorol., 90, 155–167, 1999. 9457
Stohl, A., Forster, C., Frank, A., Seibert, P., and Wotawa, G.: Technical note: The Lagrangian particle dispersion model FLEXPART version 6.2, Atmos. Chem. Phys., 5, 2461–2474, doi:10.5194/acp-5-2461-2005, 2005. 9457
Stoltzenburg, M. R. and McMurry, P. H.: An ultrafine aerosol condensation nucleus counter, Aerosol Sci. Technol., 14, 48–65, 1991. 9455
Van Dingenen, R., Putaud, J.-P., Martins-Dos Santos, S., and Raes, F.: Physical aerosol properties and their relation to air mass origin at Monte Cimone (Italy) during the first MINATROC campaign, Atmos. Chem. Phys., 5, 2203–2226, doi:10.5194/acp-5-2203-2005, 2005. 9462
Venzac, H. K., Sellegri, P., Laj, P., Villani, P., Bonasoni, A., Marinoni, P., Cristofanelli, F., Calzolari, S., Fuzzi, S., Decesari, C., Facchini, E., and Vuillermoz, G. P.: Verza, High frequency new particle formation in the Himalayas, Proc. Nat. Acad. Sci., 105, 666–671, 2008. 9464
Venzac, H., Sellegri, K., Villani, P., Picard, D., and Laj, P.: Seasonal variation of aerosol size distributions in the free troposphere and residual layer at the puy de Dôme station, France, Atmos. Chem. Phys., 9, 1465–1478, doi:10.5194/acp-9-1465-2009, 2009. 9464
Villani, P., Picard, D., Marchand, N., and Laj, P.: Design and Validation of a 6-Volatility Tandem Differential Mobility Analyzer (VTDMA), Aerosol Sci. Technol., 41, 898–906, 2007. 9455
Volkamer, R., Jimenez, J. L., San Martini, F., Dzepina, K., Zhang, Q., Salcedo, D., Molina, L. T., Worsnop, D. R., and Molina, M. J.: Secondary organic aerosol formation from anthropogenic air pollution: rapid and higher than expected, Geophys. Res. Lett., 33, L17811, doi:10.1029/2006GL026899, 2006.

ACPD
12, 9451–9490, 2012

Wang, M., Ghan, S., Easter, R., Ovchinnikov, M., Liu, X., Kassianov, E., Qian, Y., Gustafson Jr., W. I., Larson, V. E., Schanen, D. P., Khairoutdinov, M., and Morrison, H.: The multi-scale aerosol-climate model PNNL-MMF: model description and evaluation, Geosci. Model Dev., 4, 137–168, doi:10.5194/gmd-4-137-2011, 2011. 9463

Williams, J., de Reus, M., Krejci, R., Fischer, H., and Ström, J.: Application of the variability-size relationship to atmospheric aerosol studies: estimating aerosol lifetimes and ages, Atmos. Chem. Phys., 2, 133–145, doi:10.5194/acp-2-133-2002, 2002. 9453

Zhang, Q., Alfarra, M. R., Worsnop, D. R., Allan, J. D., Coe, H., Canagaratna, M. R., and Jimenez, J. L.: Deconvolution and quantification of hydrocarbon-like and oxygenated organic aerosols based on aerosol mass spectrometry, Environ. Sci. Technol., 39, 4938–4952, 2005. 9460

Zorn, S. R., Drewnick, F., Schott, M., Hoffmann, T., and Borrmann, S.: Characterization of the South Atlantic marine boundary layer aerosol using an aerodyne aerosol mass spectrometer, Atmos. Chem. Phys., 8, 4711–4728, doi:10.5194/acp-8-4711-2008, 2008. 9463, 9466, 9467

ACPD

12, 9451–9490, 2012

Table 1. Averaged meteorological parameters observed in the boundary layer (BL) and in the free troposphere (FT) for different episodes during anticyclonic (HP) and cyclonic (LP) conditions.

		RH (%)		Pot. T (K)		% of time occurring	
		HP	LP	HP	LP	HP	LP
BL	NW-EUR	64	–	102	–	33	–
	S-EUR	–	76	–	57.1	–	13
	NE-EUR	–	66	–	84.4	–	65
	E-EUR	45	22.5	92.2	87.7	67	19
	P	–	74	–	89.6	–	3
FT	NW-EUR	–	–	–	–	–	–
	S-EUR	–	54	–	61.4	–	54
	NE-EUR	–	20	–	107.8	4	23
	E-EUR	43	67	109.2	57.1	96	18
	P	–	10	–	114.5	–	5

– = Not Observed

ACPD
12, 9451–9490, 2012

Table 2. Median number concentration in the boundary layer (BL) and in the free troposphere (FT) during anticyclonic (HP) and cyclonic (LP) conditions. N_{10} : CN concentration for particles larger than 10nm measured with the CPC3010, N_{50} : CN concentration for particles larger than 50nm measured with the SMPS and N_{500} : CN concentration for particles larger than 500nm measured with the PCASP.

		N_{10} (cm^{-3})		N_{50} (cm^{-3})		N_{500} (cm^{-3})	
		HP	LP	HP	LP	HP	LP
Boundary Layer	NW-EUR	1300	–	150	–	5	–
	S-EUR	–	4800	–	5400	–	56
	NE-EUR	–	5970	–	2900	–	40
	E-EUR	5490	3135	3240	5820	28	76
	P	–	7090	–	1390	–	33
Free Troposphere	NW-EUR	–	–	–	–	–	–
	S-EUR	–	930	–	660	–	20
	NE-EUR	660	400	80	260	0	2
	E-EUR	865	920	680	940	11	29
	P	–	440	–	325	–	19

ACPD
12, 9451–9490, 2012

Table 3. Log-normal characteristics of the number size distributions shown on Figure 3. Ni represents the concentration, Di is the geometric mean diameter and σi is the standard deviation of the particle mode i (mode 1 = nucleation; mode 2 = Aitken; mode 3 = accumulation).

		HP			LP		
	Mode	Ni (cm^{-3})	Di (nm)	σi	Ni (cm^{-3})	Di (nm)	σi
				NW-EUR			
	1	186	25	1.16	–	–	–
	2	327	33.50	1.37	–	–	–
	3	138	151.2	1.6	–	–	–
				S-EUR			
	1	–	–	–	735	22.7	1.29
	3	–	–	–	6150	111.7	1.79
				NE-EUR			
	1	–	–	–	3280	28.2	1.32
	2	–	–	–	1360	56.9	1.35
BL	3	–	–	–	1750	145.8	1.63
				E-EUR			
	1	1095	25.2	1.34	–	–	–
	2	1975	59.5	1.48	5900	95	1.88
	3	1905	163.7	1.49	–	–	–
				P			
	1	–	–	–	3540	28	1.40
	3	–	–	–	1205	131	1.71
				NW-EUR			
	1	–	–	–	–	–	–
				S-EUR			
	2	–	–	–	260	40.5	1.39
	3	–	–	–	835	106.5	1.91
				NE-EUR			
	2	215	35.8	1.42	190	42.3	1.34
FT	3	45	115.9	2	220	103.6	1.70
				E-EUR			
	2	895	47	2	380	55.3	1.41
	3	605	174.8	1.52	835	141.5	1.65
				P			
	3	–	–	–	360	128	1.80

ACPD
12, 9451–9490, 2012

Table 4. Overview of total and refractory particle volume concentrations (integrated from the size distribution measurements) and volume fraction of refractory matter.

		Total volume ($\mu m^3\ cm^{-3}$)		Refractory particle volume ($\mu m^3\ cm^{-3}$)		Refractory fraction (%)	
		HP	LP	HP	LP	HP	LP
BL	NW-EUR	0.71	–	0.13	–	18	–
	S-EUR	–	47.84	–	2.90	–	6
	NE-EUR	–	8.56	–	0.82	–	9
	E-EUR	9.59	19.31	1.44	1.70	15	9
	P	–	5.32	–	0.83	–	15
FT	NW-EUR	–	–	–	–	–	–
	S-EUR	–	3.48	–	1.12	–	32
	NE-EUR	0.30	0.46	0.72	0.17	–	36
	E-EUR	4.11	3.95	0.64	1.10	15	28
	P	–	1.91	–	0.30	–	16

ACPD
12, 9451–9490, 2012

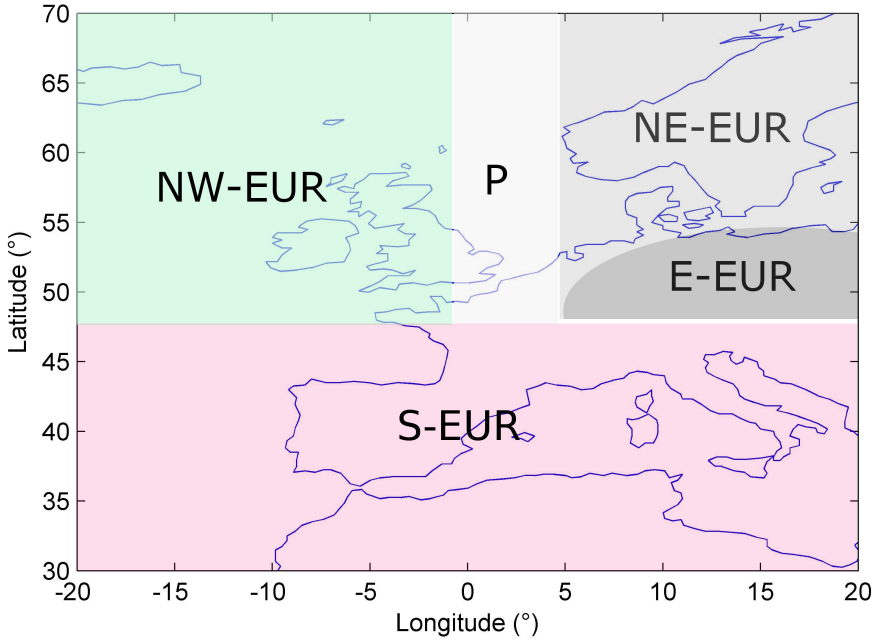

Fig. 1. Identification of the geographical sectors used for the classification of the origin of the air mass trajectories.

ACPD
12, 9451–9490, 2012

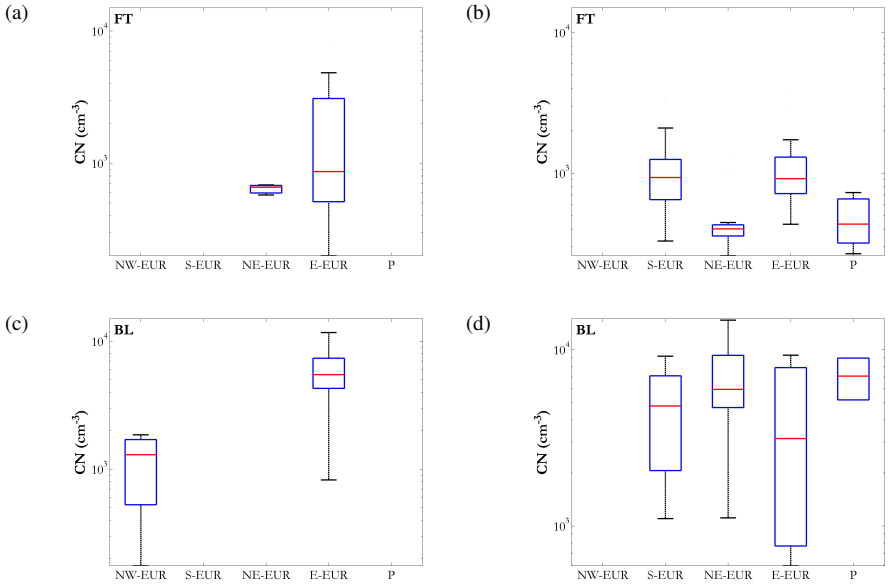

Fig. 2. Total CN concentration ($Dp > 10$ nm) as a function of the air mass origin in the free troposphere during anticyclonic **(a)** and during cyclonic **(b)** conditions as well as in the boundary layer during anticyclonic **(c)** and during cyclonic **(d)** conditions. Lower and upper limits of the box correspond to 25 % and 75 % percentiles, bottom and top whiskers the 0 % and 100 %. Middle bars indicate the median.

ACPD
12, 9451–9490, 2012

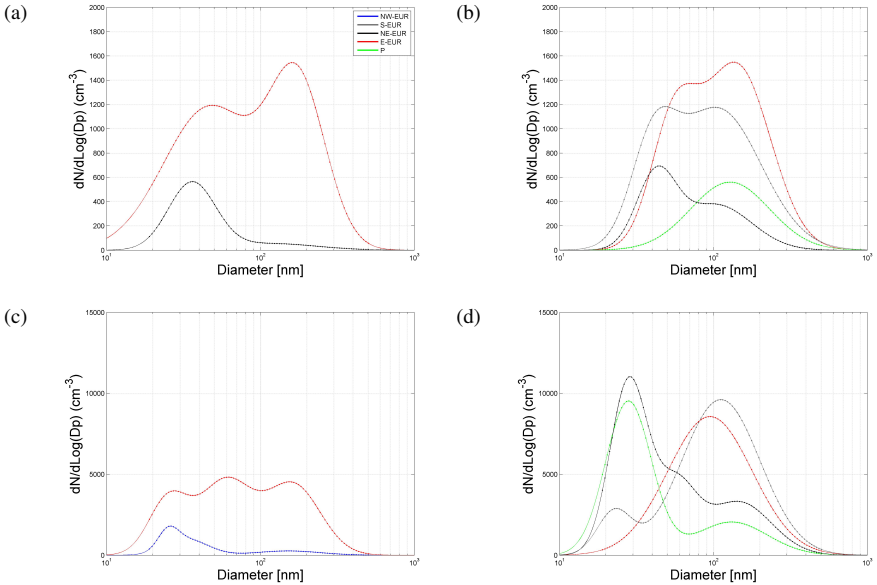

Fig. 3. Number particle size distribution (10 nm < *Dp* < 500 nm) as a function of the air mass origin in the free troposphere during anticyclonic condition **(a)** and during cyclonic condition **(b)** as well as in the boundary layer during anticyclonic condition **(c)** and during cyclonic condition **(d)**.

ACPD
12, 9451–9490, 2012

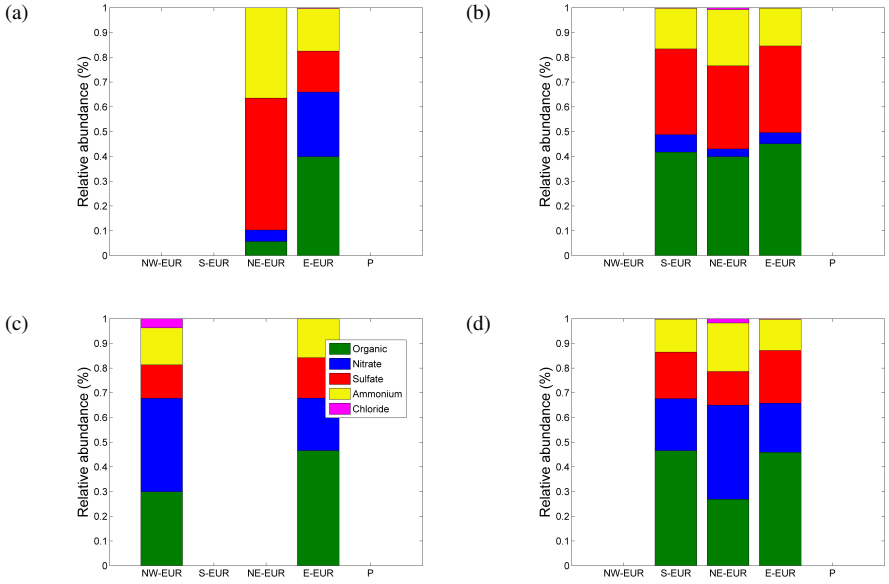

Fig. 4. Bar plot of average relative concentrations of non-refractory submicron aerosol as measured by AMS as a function of the air mass origin in the free troposphere during anticyclonic condition **(a)** and during cyclonic condition **(b)** as well as in the boundary layer during anticyclonic condition **(c)** and during cyclonic condition **(d)**.

ACPD
12, 9451–9490, 2012

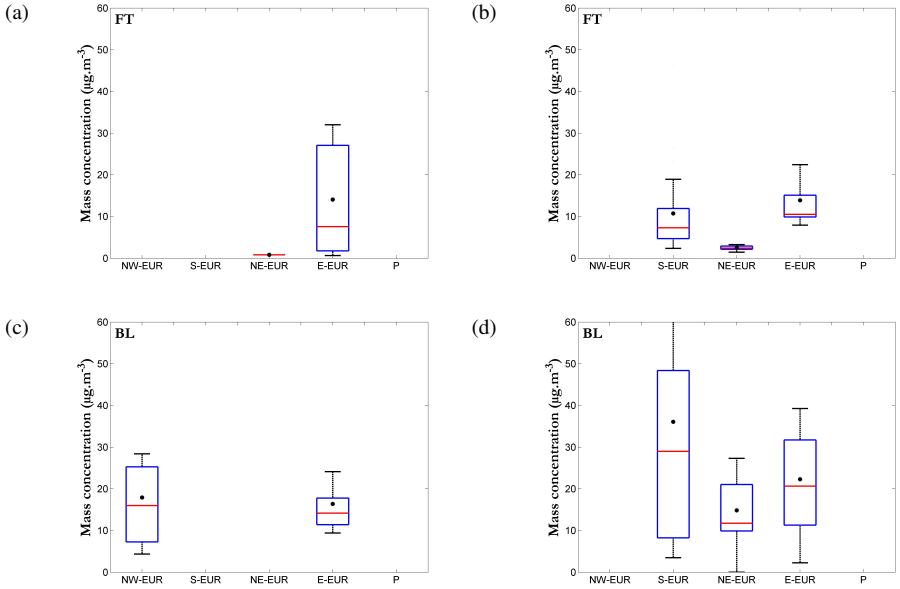

Fig. 5. Mass concentration of submicron non-refractory aerosol as measured by AMS as a function of the air mass origin in the free troposphere during anticyclonic condition **(a)** and during cyclonic condition **(b)** as well as in the boundary layer during anticyclonic condition **(c)** and during cyclonic condition **(d)**. Lower and upper limits of the box correspond to 25 % and 75 % percentiles, bottom and top whiskers the 0 % and 100 %. Middle bars indicate the median. Black points represent the total mass concentration (including the mass of refractory material derived from its volume distribution and a density of 1.8 g cm^{-3}).

ACPD
12, 9451–9490, 2012

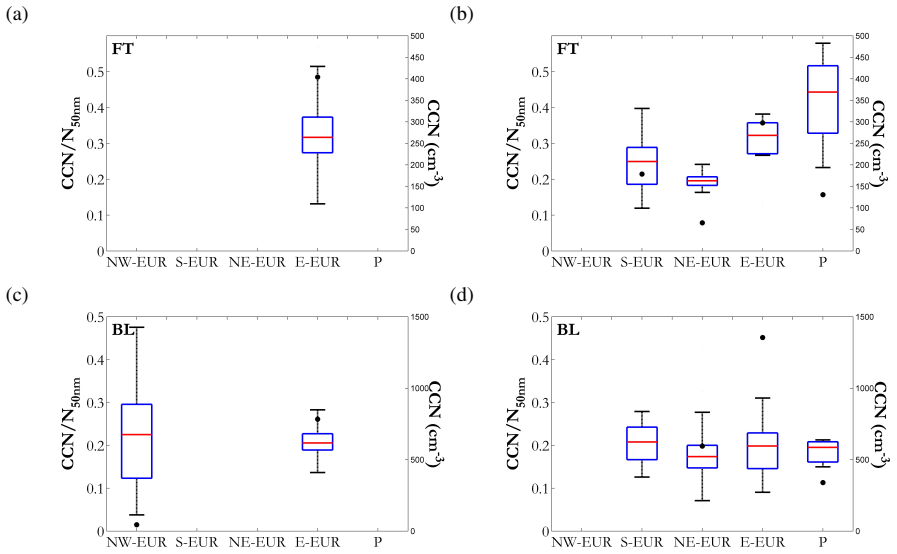

Fig. 6. CCN/N_{50} ratio (left scale) as a function of the air mass origin in the free troposphere during anticyclonic condition **(a)** and during cyclonic condition **(b)** as well as in the boundary layer during anticyclonic condition **(c)** and during cyclonic condition **(d)**. Black points represent the median CCN concentration (right scale).

ACPD
12, 9451–9490, 2012

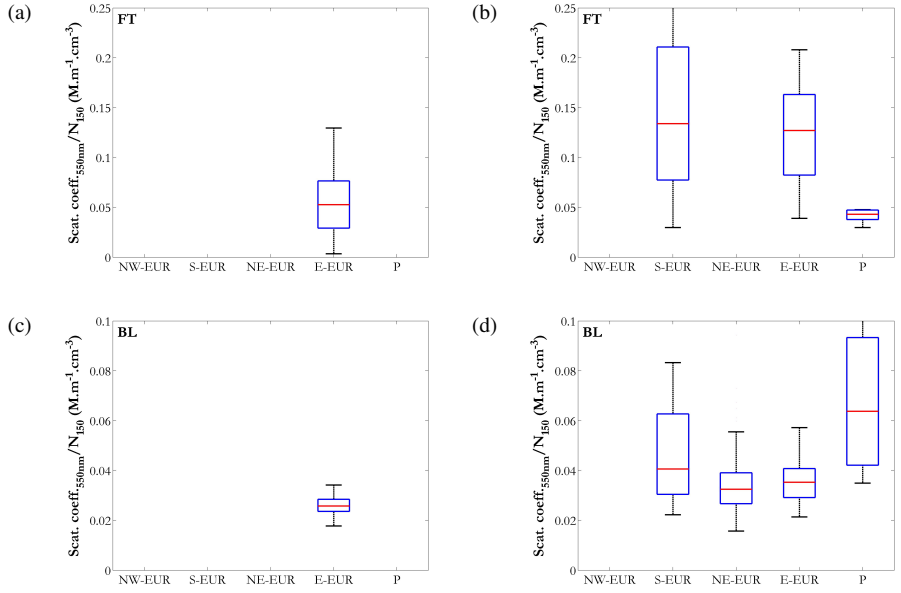

Fig. 7. Scattering cross-section calculated at 550nm for particles larger than 150 nm as a function of the air mass origin in the free troposphere during anticyclonic condition **(a)** and during cyclonic condition **(b)** as well as in the boundary layer during anticyclonic condition **(c)** and during cyclonic condition **(d)**. Lower and upper limits of the box correspond to 25 % and 75 % percentiles, bottom and top whiskers the 0 % and 100 %. Middle bars indicate the median.

ACPD
12, 9451–9490, 2012

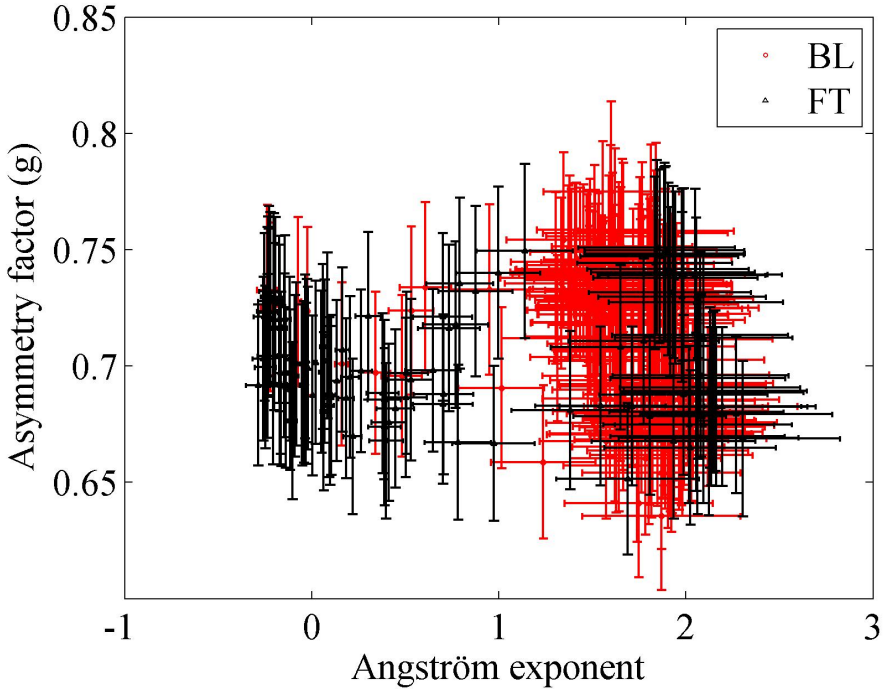

Fig. 8. Asymmetry factor as a function of the scattering Angström coefficient both obtained from the nephelometer measurements (at 550 nm) in the boundary layer (red circles) and in the free troposphere (black triangles).

ACPD
12, 9451–9490, 2012